Orbital magnetization and anomalous Hall effect in interacting Weyl semimetals

S. Acheche,[1] R. Nourafkan,[1] and A.-M. S. Tremblay[1,2,*]

[1]*Département de physique, Institut quantique, and Regroupement québécois sur les matériaux de pointe, Université de Sherbrooke, Sherbrooke, Québec, Canada J1K 2R1*

[2]*Canadian Institute for Advanced Research, Toronto, Ontario, Canada M5G 1Z8*

(Received 19 July 2018; published 22 February 2019)

Ferromagnetic Weyl semimetals exhibit an anomalous Hall effect, a consequence of their topological properties. In the noninteracting case, the derivative of the orbital magnetization with respect to chemical potential is proportional to this anomalous Hall effect, the Středa formula. Motivated by compounds such as Mn_3Sn, here we investigate how interactions modeled by a Hubbard U impact on both quantities when the Fermi energy is either aligned with the Weyl nodes or away from them. Using dynamical mean-field theory, we first find interaction-induced Mott- and band-insulating transitions. In the Weyl semimetal regime, away from insulators, interactions lead to an increase in the imbalance between the densities of spin species induced by a Zeeman term h. This increased imbalance leads to an increase of the anomalous Hall effect that can also be understood from the displacement of the Weyl nodes and topological arguments. This interaction-induced spin imbalance also compensates the reduction in orbital magnetization of each spin species that comes from smaller quasiparticle weight. In the small interaction regime, the combined effects lead to an orbital magnetization that depends weakly on interaction and still changes linearly with chemical potential at small doping. In the intermediate and strong correlation regimes, the localization due to interaction affects strongly the orbital magnetization, which becomes small. A quasiparticle picture explains the anomalous Hall effect but does not suffice for the orbital magnetization. We propose a modified Středa formula to relate anomalous Hall effect and orbital magnetization in the weak correlation limit. We also identify mirror and particle-hole symmetries of the lattice model that explain, respectively, the vanishing of the anomalous Hall effect at $h = 0$ for all U and μ of the orbital magnetization at half-filling $\mu = 0$ for all U and h.

DOI: 10.1103/PhysRevB.99.075144

I. INTRODUCTION

Weyl semimetals are three-dimensional (3D) topological materials in which two nondegenerate energy bands touch at isolated wave vectors (Weyl nodes) [1,2]. The electronic structure near the Weyl nodes is described by linearly dispersive bands. The nondegenerate bands are a consequence of either time-reversal or inversion symmetry breaking. The Weyl physics governs the transport properties when the Fermi energy lies on, or in the vicinity, of the Weyl nodes. For instance, a subclass of Weyl semimetals named ferromagnetic (FM) Weyl metals demonstrates a nonzero anomalous Hall effect (AHE) [3,4].

The AHE is not a specific property of FM Weyl metals since every FM conductor can potentially exhibit a nonzero transverse conductivity which is not related to an external magnetic field [5]. Two main contributions to the Hall conductivity are (i) an intrinsic AHE that comes from Berry curvature and (ii) an extrinsic AHE due to scattering on impurities in the presence of spin-orbit coupling [5]. In general, both contributions are present with the same order of magnitude, but for FM Weyl metals the intrinsic AHE tends to dominate the extrinsic part even if the chemical potential does not lie exactly on the Weyl nodes [3]. This theoretical assertion has found a possible experimental evidence recently with the Weyl ferromagnet $Co_3Sn_2S_2$ [6].

A nonzero Berry curvature not only influences transport properties but also impacts properties such as orbital magnetization [7–13]. Indeed, in a noninteracting system the Středa formula [14] links the orbital magnetization and intrinsic AHE, the latter being proportional to the derivative of the magnetization with respect to the chemical potential. In the case of FM Weyl metals, the Středa formula suggests the common origin of the two quantities: both owe their existence to stacks of two-dimensional Chern insulators in momentum space [8,15].

How electronic correlations impact the AHE and orbital magnetization of Weyl semimetals is the subject of this study. In particular, recent experimental evidence has shown Weyl physics in the presence of bands that are strongly renormalized by interactions [16]. For instance, the Weyl material Mn_3Sn [16], an antiferromagnet with weak ferromagnetism, is known to exhibit a large AHE even at room temperature [17]. All this motivates our study of the interplay between electron-electron interactions and topological properties of Weyl semimetals.

Theoretically, interacting Weyl semimetals have been studied through various methods, such as random phase approximation [18], renormalization group [19,20], and Hubbard interaction through cluster methods [21,22]. The focus of attention was broken-symmetry phases, band renormalization,

*Corresponding author: andre-marie.tremblay@usherbrooke.ca

TABLE I. Location and chirality of the four Weyl nodes for $|h| < 2t$.

Chirality		
-1	$(\pi, 0, +\arccos(h/2t))$	$(0, \pi, +\arccos(h/2t))$
$+1$	$(\pi, 0, -\arccos(h/2t))$	$(0, \pi, -\arccos(h/2t))$

or stability of Weyl nodes under the effect of electron-electron interaction. In this paper, we investigate how interactions represented by a Hubbard U on a lattice model of Weyl semimetals impact on the AHE and on orbital magnetization of the FM Weyl semimetal. We show how the Středa formula is changed due to the presence of interaction and how many of the results can be explained from a quasiparticle perspective. We also find that because of competing effects, the orbital magnetization is rather insensitive to interactions near half-filling, even though it is not a purely topological quantity. We briefly discuss also the semimetal-to-insulator transition at large U.

The model and method are presented in Sec. II. Section III introduces various properties of interacting Weyl semimetals, in particular how the metal-insulator transition occurs either through Mott physics or through Weyl-node collapse. In Sec. IV, we compute the Hall conductivity to see how it changes as a function of interaction. A quasiparticle (QP) approach is derived in order to capture this change in a single-particle formalism. Finally, Sec. V is devoted to the orbital magnetization. We check the validity of the Středa formula for our model in the noninteracting case and suggest how to modify this formula in the presence of the Hubbard interaction. The QP approach and perturbation theory are used there again to understand quantitatively the interacting case.

II. MODEL AND METHOD

We use a lattice model of Weyl semimetals with Hubbard interaction on a cubic lattice. The model is simple and is usually considered as a generic model for time-reversal symmetry-breaking Weyl semimetals [23]. We will see, however, that it has some symmetries that are not obvious at first sight. The full Hamiltonian is

$$\hat{H} = \hat{H}_0 + U \sum_{\mathbf{r}} \left(\hat{n}_{\mathbf{r}\uparrow} - \frac{1}{2}\right)\left(\hat{n}_{\mathbf{r}\downarrow} - \frac{1}{2}\right) - \mu \sum_{\mathbf{r}} \hat{n}_{\mathbf{r}}, \quad (1)$$

where U is the Hubbard interaction term, μ is the chemical potential, and $\hat{H}_0$ denotes the noninteracting part of the Hamiltonian. Its momentum-space expression is [23]

$$\hat{H}_0 = \sum_{\mathbf{k}} \hat{\mathbf{C}}^{\dagger}_{\mathbf{k}} [\{h - 2t(\cos k_x + \cos k_y + \cos k_z)\}\boldsymbol{\sigma}_z + 2t \sin k_y \boldsymbol{\sigma}_y + 2t \sin k_x \boldsymbol{\sigma}_x] \hat{\mathbf{C}}_{\mathbf{k}}. \quad (2)$$

Here, t denotes the nearest-neighbor hopping amplitude and h is a Zeeman term. We set $t = 1$ as energy unit and use Hartree units ($\hbar = e = k_B = 1$). The destruction (creation) operator $\hat{\mathbf{C}}_{\mathbf{k}} = (\hat{c}_{\mathbf{k}\uparrow}, \hat{c}_{\mathbf{k}\downarrow})^{(T)}$ is represented in the spin basis and $\boldsymbol{\sigma}_i$ are Pauli matrices. For those values of h used in this paper, there are four Weyl nodes whose location and chirality are indicated in Table I.

TABLE II. Effect of elementary transformations on the destruction operators along with their effect on χ and on the the spin eigenstates of $\sigma_{x,y,z}$. P is parity, T time reversal, C' pseudo-charge conjugation, $\mathcal{T}_{\mathcal{Q}}$ translation by $\mathcal{Q} = (\pi, \pi, \pi)$, and $\mathcal{M}_{zx/zy}$ mirrors across the specified plane. Summation over repeated σ' is implied.

Discrete transformations	χ	σ_x	σ_y	σ_z
$P\hat{c}_{\mathbf{k}\sigma}P^{-1} = \hat{c}_{-\mathbf{k}\sigma}$	-1	$+1$	$+1$	$+1$
$T\hat{c}_{\mathbf{k}\sigma}T^{-1} = i\sigma^{y}_{\sigma\sigma'}\hat{c}_{-\mathbf{k}-\sigma'}$	-1	-1	-1	-1
$C'\hat{c}_{\mathbf{k}\sigma}C'^{-1} = \hat{c}^{\dagger}_{\mathbf{k}\sigma}$	$+1$	-1	-1	-1
$\mathcal{T}_{\mathbf{Q}}\hat{c}_{\mathbf{k}\sigma}\mathcal{T}_{\mathbf{Q}}^{-1} = \hat{c}_{\mathbf{k}+\mathbf{Q}\sigma}$	-1	$+1$	$+1$	$+1$
$\mathcal{M}_{zy}\hat{c}_{\mathbf{k}\sigma}\mathcal{M}_{zy}^{-1} = \sigma^{x}_{\sigma\sigma'}\hat{c}_{(-k_x,k_y,k_z)\sigma'}$	-1	$+1$	-1	-1
$\mathcal{M}_{zx}\hat{c}_{\mathbf{k}\sigma}\mathcal{M}_{zx}^{-1} = i\sigma^{y}_{\sigma\sigma'}\hat{c}_{(k_x,-k_y,k_z)\sigma'}$	-1	-1	$+1$	-1

The Hamiltonian has several symmetries that will help us later to understand the physics of the results. First, let us define elementary discrete transformations that have eigenvalues ± 1: parity P, time reversal T, translation $\mathcal{T}_{\mathbf{Q}}$ by $\mathbf{Q} = (\pi, \pi, \pi)$, xz mirror $\mathcal{M}_{xz}$, and yz mirror $\mathcal{M}_{yz}$. Note that $\mathcal{T}_{\mathbf{Q}}$ reflects the bipartite nature of the lattice. We also define a pseudo-charge-conjugation transformation C' analogous to, but different from, the one that usually appears in field theory [24]. The effect of these elementary transformations on the destruction operators and their eigenvalues for chirality and spin components of the noninteracting Hamiltonian (2) in the case $h = 0$ are tabulated in Table II. The transformations act on the same way on the labels of the creation operators.

Using these results, we find that when $\mu = 0$, the following symmetry operation,

$$(C'PT)\hat{c}_{\mathbf{k}\sigma}(C'PT)^{-1} = i\sigma^{y}_{\sigma\sigma'}\hat{c}^{\dagger}_{\mathbf{k}\sigma'}, \quad (3)$$

is a particle-hole transformation that leaves Eq. (1) invariant for all U, and h. Since under this symmetry operation $\hat{n}_{\sigma} \to 1 - \hat{n}_{-\sigma}$, this means that $\mu = 0$ corresponds to half-filling.

When $h = 0$, but for arbitrary values of μ and U, there are two more symmetries of $\hat{H}$ that we will call *translated mirrors*, for lack of a better name:

$$(\mathcal{T}_{\mathbf{Q}}\mathcal{M}_{zy})\hat{c}_{\mathbf{k}\sigma}(\mathcal{T}_{\mathbf{Q}}\mathcal{M}_{zy})^{-1} = \sigma^{x}_{\sigma\sigma'}\hat{c}_{(-k_x+\pi,k_y+\pi,k_z+\pi)\sigma'}, \quad (4)$$

$$(\mathcal{T}_{\mathbf{Q}}\mathcal{M}_{zx})\hat{c}_{\mathbf{k}\sigma}(\mathcal{T}_{\mathbf{Q}}\mathcal{M}_{zx})^{-1} = i\sigma^{y}_{\sigma\sigma'}\hat{c}_{(k_x+\pi,-k_y+\pi,k_z+\pi)\sigma'}. \quad (5)$$

In this paper, the fully interacting system is solved within the dynamical mean-field theory (DMFT) framework [25]. In this theory, the system is mapped onto an interacting quantum impurity site hybridized with a bath of noninteracting electrons. The lattice self-energy is the same as the impurity self-energy. The hybridization function between the impurity and the bath is then determined self-consistently by imposing equality of the impurity Green's function and the projection of the lattice Green's function on a single site. Although the method is exact only in the limit of infinite dimension, it has been very successful in describing the physics of three-dimensional systems. To obtain the impurity Green's function, a finite-temperature exact diagonalization (ED) solver [26] is used. For an ED solver, the noninteracting electron bath is represented by a finite number of bath *sites* hybridized with the impurity. The impurity problem is then solved exactly by diagonalizing numerically the Hamiltonian. In ED, the self-consistency condition is partially

respected by minimizing with respect to the bath parameters the mean-square distance between the hybridization function obtained from Dyson equation and the one written in terms of bath parameters [26]. We usually keep 1024 Matsubara frequencies. The convergence criterion is 2×10^{-5} on a relative scale. All numerical computations are done at inverse temperature $\beta = 80$ and with five bath sites. Increasing the number of bath sites should lead to more quantitatively accurate results but should not change our conclusions. The main effect of the finite number of bath sites is that real-frequency quantities are represented by a set of closely spaced delta functions. We will see a consequence of that in the next section. The spacing increases at larger frequencies. However, quantities in Matsubara frequencies, which is all that we need for thermodynamic quantities such as orbital magnetization and AHE, remain smooth functions that are accurately represented by the finite number of bath sites.

III. INTERACTING WEYL SEMIMETAL AND MOTT TRANSITION

In this section we discuss how interactions impact the dynamics of the Weyl electrons, first in the absence of a Zeeman coupling ($h = 0$). At a finite value of U, several of the changes occurring in the system manifest themselves in the density of states (DOS). In Fig. 1, we show the DOS for both noninteracting and interacting Weyl semimetals. In the noninteracting case, two regions can be defined: Near the Fermi level, i.e., for $-2 \lesssim \omega \lesssim 2$, electronic bands are mainly linear and we recover the DOS of three-dimensional (3D) semimetals characterized by ω^2 behavior. Outside this region, the dispersion is not linear anymore and the DOS eventually retains the characteristics of the cubic lattice DOS. In the presence of the Hubbard interaction, band energies are renormalized leading to a narrower DOS near the Fermi level and to Hubbard band satellites. The renormalization

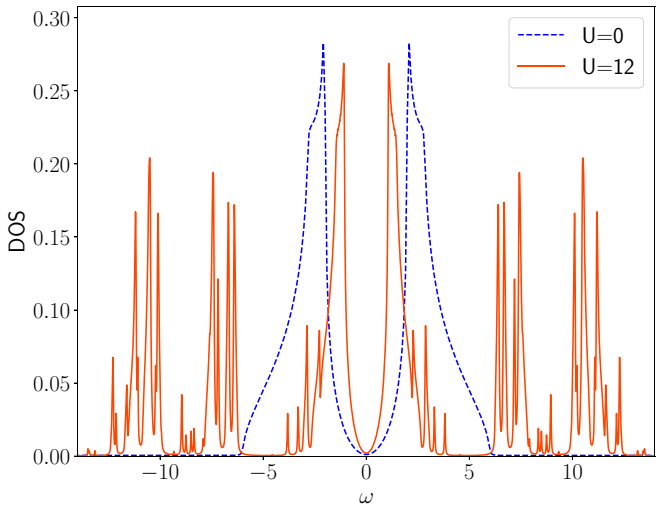

FIG. 1. (a) Density of states for noninteracting (dashed blue line) and interacting (continuous red line) Weyl semimetals. $U = 12$ corresponds to the bandwidth of the model (2). Sharp peaks are due to the finite number of bath sites of the DMFT impurity solver. We use a Lorentzian broadening $\eta = 0.02$ for both densities of states.

factor is given by the bulk quasiparticle weight defined as $\boldsymbol{Z} \simeq [\mathbf{I} - \mathrm{Im}\boldsymbol{\Sigma}(i\omega_0)/\omega_0]^{-1}$, where $\boldsymbol{\Sigma}$ denotes the Matsubara self-energy and $\omega_0 = \pi/\beta$ is the first fermionic Matsubara frequency. In our system at half-filling, $\boldsymbol{Z}$ is a diagonal matrix with $Z_{\uparrow\uparrow} = Z_{\downarrow\downarrow} = Z$. Hence, the low-energy effective Hamiltonian describing the Weyl fermion physics is obtained from the noninteracting one by substituting for the velocity tensor $v_{ij} \to Zv_{ij}$. Note that the incoherent part (Hubbard bands) does not contribute to transport properties, so a renormalized noninteracting low-energy Hamiltonian should be a good approximation for determining these properties.

As expected, the lower and upper Hubbard bands form, respectively, at $\omega = -U/2$ and $U/2$ by transferring spectral weight to high energy. At $U_{c2} \approx 19.5$, the system undergoes a phase transition from a semimetal to a Mott-insulating phase. The Mott phase has trivial topology with a large charge gap and is characterized by the emergence of a diverging self-energy at low Matsubara frequencies. The Mott transition occurs when the Hubbard interaction is large enough to localize electrons on lattice sites. It is worth mentioning that the interaction does not shift Weyl nodes when $h = 0$ even away from half-filling. This property is not related to the locality of the DMFT self-energy but rather symmetries of the microscopic model, as we discuss below. In other lattice models, e.g., in Refs. [21,22], Weyl-node positions depend on the prefactor of $\boldsymbol{\sigma}_x$. In this case, the Fock diagram shifts Weyl nodes in the same way as the Hartree diagram shifts nodes in our case when h is finite. Indeed, in the finite-h case, the Weyl-node locations in our model depend on the prefactor h of $\boldsymbol{\sigma}_z$ in the noninteracting Hamiltonian. A finite value of h leads to a self-energy proportional to $\boldsymbol{\sigma}_z$ that changes this prefactor.

We can understand the above results with the help of symmetries. In the absence of a Zeeman term ($h = 0$), the translated mirror symmetries (4) and (5) fix the position of Weyl nodes in the Brillouin zone. Since these symmetries hold independently of the electronic density of the system, the Weyl nodes are fixed also away from half-filling. A finite Zeeman term h breaks those symmetries and makes the position of Weyl nodes interaction dependent.

The shift in position of Weyl nodes in the presence of a finite h leads to two different scenarios for the insulating phases in the strong correlation regime [27]: on one hand, if U becomes large enough before merging of the Weyl nodes, the system goes to the Mott-insulating phase as in the case $h = 0$. On the other hand, if Weyl nodes merge before the Mott transition, the system becomes a *band insulator* characterized by full spin polarization. Since only one species of spin is present once this semimetal to band-insulator transition occurs, the Hubbard interaction has no effect anymore, regardless of the value of U.

IV. ANOMALOUS HALL EFFECT

The anomalous Hall conductivity σ_{xy} is a dissipation-less transverse current response to an electric field. It is given by the first-order expansion in powers of frequency of the corresponding current-current correlation function Π_{xy} in frequency. In contrast to an Ohmic (dissipative) response, the frequency expansion can be done on the imaginary axis [28]. Using the standard formula for the polarization Π_{xy} [29], we

have

$$\Pi_{xy}(i\nu_n) = -\frac{1}{N\beta}\sum_{\mathbf{k}\omega_m}\mathrm{Tr}\left[v_x(\mathbf{k})\boldsymbol{G}(i\omega_m+i\nu_n,\mathbf{k})\frac{\partial \boldsymbol{G}^{-1}(i\omega_m,\mathbf{k})}{\partial k_y}\boldsymbol{G}(i\omega_m,\mathbf{k})\right] \tag{6}$$

$$\approx \Pi_{xy}(0) + \underbrace{\frac{1}{N\beta}\sum_{\mathbf{k}\omega_m}\mathrm{Tr}\left[\frac{\partial \boldsymbol{G}^{-1}(i\omega_m,\mathbf{k})}{\partial k_x}\boldsymbol{G}(i\omega_m,\mathbf{k})\frac{\partial \boldsymbol{G}^{-1}(i\omega_m,\mathbf{k})}{\partial i\omega_n}\boldsymbol{G}(i\omega_m,\mathbf{k})\frac{\partial \boldsymbol{G}^{-1}(i\omega_m,\mathbf{k})}{\partial k_y}\boldsymbol{G}(i\omega_m,\mathbf{k})\right]}_{\text{first order}} i\nu_n + \cdots,$$

where ν_n denotes bosonic Matsubara frequencies. The velocity operators are defined as $v_i = -\partial_{k_i}\boldsymbol{H}_0$ and $\boldsymbol{G}$ is the interacting Green's function given by

$$\boldsymbol{G}(i\omega_n,\mathbf{k}) = [(i\omega_n+\mu)\mathbf{I} - \boldsymbol{H}_0(\mathbf{k}) - \boldsymbol{\Sigma}(i\omega_n)]^{-1}. \tag{7}$$

In DMFT, the self-energy has only frequency dependence, hence, the derivatives of inverse Green's functions with respect to wave vectors reduce to velocity operators without vertex corrections. However, the derivative of the self-energy with respect to frequency is taken into account.

The nontrivial band topology of a FM Weyl semimetal gives a finite AHE which can be understood as follows; in reciprocal space, each Weyl node can be seen as the position of a *magnetic* monopole, where the associated magnetic field is the Berry curvature [30]. Assuming only two Weyl nodes with opposite chirality separated by a vector $\mathbf{b}$ in the first Brillouin zone, the region between nodes can be decomposed as a stack of two-dimensional (2D) Chern insulators. Each of these insulators carries a nonzero Chern number C corresponding to the flux of the Berry curvature in a plane and contributes to the anomalous conductivity [15,31–34]. For example, if $\mathbf{b}$ is along the z direction, then the AHE in the z direction is given by

$$\sigma_{xy} = \frac{Cb}{2\pi^2}, \tag{8}$$

which depends only on the Weyl-node separation in wave-vector space. In systems with several Weyl nodes, one can define an effective vector $\mathbf{b}_{\text{eff}} = \sum_i \chi_i \mathbf{b}_i$, where the sum is over all Weyl nodes in the first Brillouin zone and χ_i is the chirality of the i the Weyl node located at $\mathbf{b}_i$ with respect to an arbitrary origin.[1]

As presented in Table I, Eq. (2) has four Weyl nodes in the Brillouin zone located at $(0,\pi,\pm\arccos(h/2t))$ and $(\pi,0,\pm\arccos(h/2t))$. In the absence of Zeeman coupling $(h=0)$, the $\mathbf{b}_{\text{eff}}$ vector is $(0,0,2\pi)$, which is equivalent to a vanishing effective vector, yielding zero anomalous Hall conductivity. Moreover, one can show by contradiction that at $h=0$ the translated mirror symmetries (4) and (5) fix the position of the Weyl nodes to $(0,\pi,\pm\pi/2)$ and $(\pi,0,\pm\pi/2)$ even when interactions U are present, hence, the AHE vanishes also in this case.

Alternatively, using an effective Hamiltonian where lattice effects are kept only in the z direction (see Appendix A), when $h=0$ the intrinsic part of anomalous Hall conductivity is given by (assuming the chemical potential lies on the node)

$$\tilde{\sigma}_{xy} = -\int dk_z d^2q \frac{2t^2[-2t\cos(k_z)]}{\left([2t\cos(k_z)]^2 + 4t^2q_x^2 + 4t^2q_y^2\right)^{\frac{3}{2}}}, \tag{9}$$

where q_x and q_y denote wave vectors with respect to the Weyl-node location in the Brillouin zone. As one can see, integrating on k_z leads to a vanishing AHE.

A Zeeman term $h\neq 0$ creates a spin-polarized FM Weyl metal, i.e., a Weyl semimetal where the densities of spin species are not equal to each other ($\langle n_\uparrow\rangle \neq \langle n_\downarrow\rangle$). In addition to that, h changes the position of the Weyl nodes in the Brillouin zone, leading also to a nonzero $\mathbf{b}_{\text{eff}}$ and a finite AHE.

In the presence of a finite h, let us consider the noninteracting and interacting cases in turn. At $U=0$, one can use the same effective Hamiltonian as in Eq. (9) to compute the anomalous Hall conductivity and find (cf. Appendix A)

$$\sigma_{xy} = (-1/\pi^2)\arcsin\left(\frac{h}{2t}\right). \tag{10}$$

Note, however, that the spin-density imbalance is also the key to understand AHE in FM compounds and thus the AHE cannot be attributed to a specific property of Weyl metals.

At finite U we find an effect on the AHE even at half-filling. Figure 2(a) shows the change of the Hall conductivity as a function of Hubbard interaction. One recovers the value given by Eq. (10) when $U=0$. Upon increasing $U>0$, the (absolute value of) the Hall conductivity increases monotonously [21] despite a reduction in coherent spectral weight. Indeed, due to its particular form, the Hubbard interaction increases the difference between electronic densities of each spin species leading to an enhanced effective h and, consequently, to a larger value of the AHE. Increasing U for a fixed h, the anomalous Hall conductivity keeps increasing until the critical U for the Mott transition where it falls to zero discontinuously.

The change in the anomalous Hall conductivity can be quantitatively understood within the QP approximation (see Appendix B for more details). With this approximation, the QP Hamiltonian is

$$\boldsymbol{H}^{\text{QP}} = \boldsymbol{Z}^{1/2}[\boldsymbol{H}_0 - \mu\mathbf{I} + \mathrm{Re}\boldsymbol{\Sigma}(\omega=0)]\boldsymbol{Z}^{1/2}, \tag{11}$$

where $\boldsymbol{Z}$ is the quasiparticle weight. In the presence of h, interaction changes the location of the Weyl nodes to $(0,\pi,\pm\arccos((h+\Sigma^z)/2t))$ and $(\pi,0,\pm\arccos((h+\Sigma^z)/2t))$ leading to a $\mathbf{b}_{\text{eff}}$ vector that depends on U. Figure 2 shows the change of the AHE as a function of $\tilde{h} = h + \Sigma^z$ for different values of h: the black continuous line is the

[1]One has to be careful not substitute blindly $\mathbf{b}_{\text{eff}}$ in Eq. (8). The periodicity of the Brillouin zone in lattice models needs to be taken into account. This explains the absence of the AHE in our case when $h=0$.

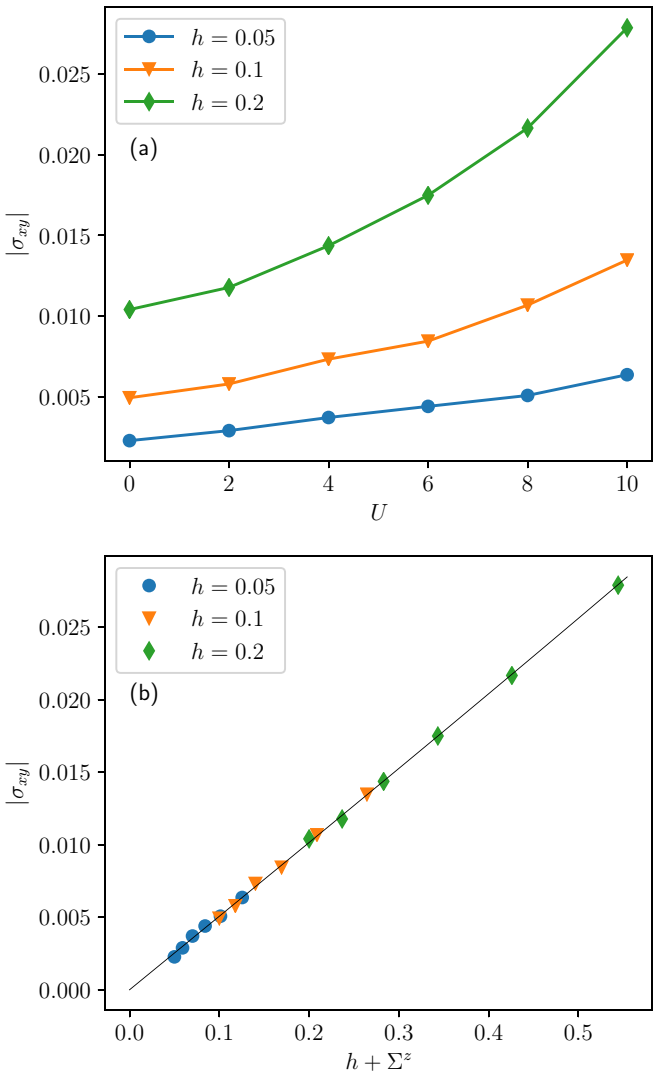

FIG. 2. (a) Anomalous Hall conductivity as a function of U at half-filling. (b) Anomalous Hall conductivity as a function of the renormalized Zeeman term $\tilde{h} = h + \Sigma^z$. The continuous black line is the theoretical value found by replacing h by $\tilde{h}$ in Eq. (10).

theoretical value presented in Eq. (10) with h replaced by $\tilde{h}$. There is a fine agreement between the analytic expression and numerical computation for a wide range of U.

To understand the expression for $\tilde{h}$, the self-energy at zero frequency has then been rewritten as $\mathrm{Re}\boldsymbol{\Sigma}(\omega = 0) = \Sigma^{\mathrm{I}}\mathbf{I} + \Sigma^z\boldsymbol{\sigma}^z$. Here, $\Sigma^{\mathrm{I}} = (\Sigma_{\uparrow\uparrow} + \Sigma_{\downarrow\downarrow})/2$ and $\Sigma^z = (\Sigma_{\uparrow\uparrow} - \Sigma_{\downarrow\downarrow})/2$. We performed a perturbative calculation and found that at low to intermediate interaction strengths, Σ^{I} is well described by second-order perturbation theory. However, describing Σ^z requires higher-order perturbation theory.

Away from half-filling, there are contributions to the anomalous Hall effect that are not purely topological even in the noninteracting case, so we do not consider the $n \neq 1$ case.

V. ORBITAL MAGNETIZATION

The impact of nontrivial topology on orbital magnetic susceptibility has been intensively studied [35–41]. Here, we focus on orbital magnetization, a quantity closely related to the AHE. The orbital magnetization is defined by $M^a_{\mathrm{orb}} = -\partial(E - \mu N)/\partial B|_{T=0,B=0}$, where E is the energy of the system. In general, it can be written in terms of the fully interacting Green's function [9] and is approximately given by

$$M^a_{\mathrm{orb}} \simeq \left(\frac{i}{2N\beta}\right) \sum_{\mathbf{k}, i\omega_m} \epsilon^{abc}\mathrm{Tr} \times \left\{ \underbrace{\left[\boldsymbol{H}_0 - \mu\mathbf{I} + \frac{\boldsymbol{\Sigma}}{2}\right]}_{\text{energy vertex}} \boldsymbol{G}\left(-\frac{\partial \boldsymbol{G}^{-1}}{\partial k_b}\right)\boldsymbol{G}\left(-\frac{\partial \boldsymbol{G}^{-1}}{\partial k_c}\right)\boldsymbol{G} \right\}. \tag{12}$$

In Eq. (12), ϵ^{abc} is the fully antisymmetric Levi-Civita tensor and a, b, and c are spatial coordinates ($\{x, y, z\}$). In the paradigm of a purely local self-energy, this formula takes into account both kinetic and potential energy contributions correctly. Indeed, we neglected an additive term proportional to the linear response of the self-energy to the magnetic field, but this term vanishes in the DMFT approximation.

It is important to stress that this formula reduces to *the modern theory of the orbital magnetization* [7,8] when the self-energy is set to zero (cf. Appendix A of Ref. [9]). This fact indicates that the above general formula takes into account topological contributions even in the presence of correlations. The formula is derived in the limit of zero external magnetic field. However, we use it in the presence of a small Zeeman term entering H_0. This should be correct if the Zeeman term is sufficiently small or if it arises from spontaneous symmetry breaking. We also neglect the spin contribution to the magnetic field and focus on the z component of the orbital magnetization.

We consider in turn the noninteracting case, where we recover the Středa formula that relates anomalous Hall effect and orbital magnetization, and the interacting case, where strong deviations are found.

A. Orbital magnetization for the noninteracting case

Similar to the AHE, the orbital magnetization is nonzero only in the presence of a finite h. In order to understand how a finite h leads to a finite orbital magnetization, we look at the contribution of each component (partial magnetization) to the trace in Eq. (12). Figure 3(a) shows the partial orbital magnetizations. As one can see, the partial orbital magnetizations are nonzero even at $h = 0$ but they have opposite signs, canceling each other at $h = 0$. At finite h, the exact cancellation between the partial orbital magnetizations disappears, leading to finite orbital magnetization. However, in the model (1), the particular form of partial orbital magnetization and the fact that the shift is symmetrical around $\mu = 0$ imposes zero orbital magnetization for $\mu = 0$, regardless of the value of h. In terms of symmetries, even if the Green's function part of the orbital magnetization (12) is affected at finite h, the particle-hole symmetry (3) is still present when $\mu = 0$. The presence of the energy vertex and particle-hole symmetry then implies that the orbital magnetization vanishes at $\mu = 0$ even

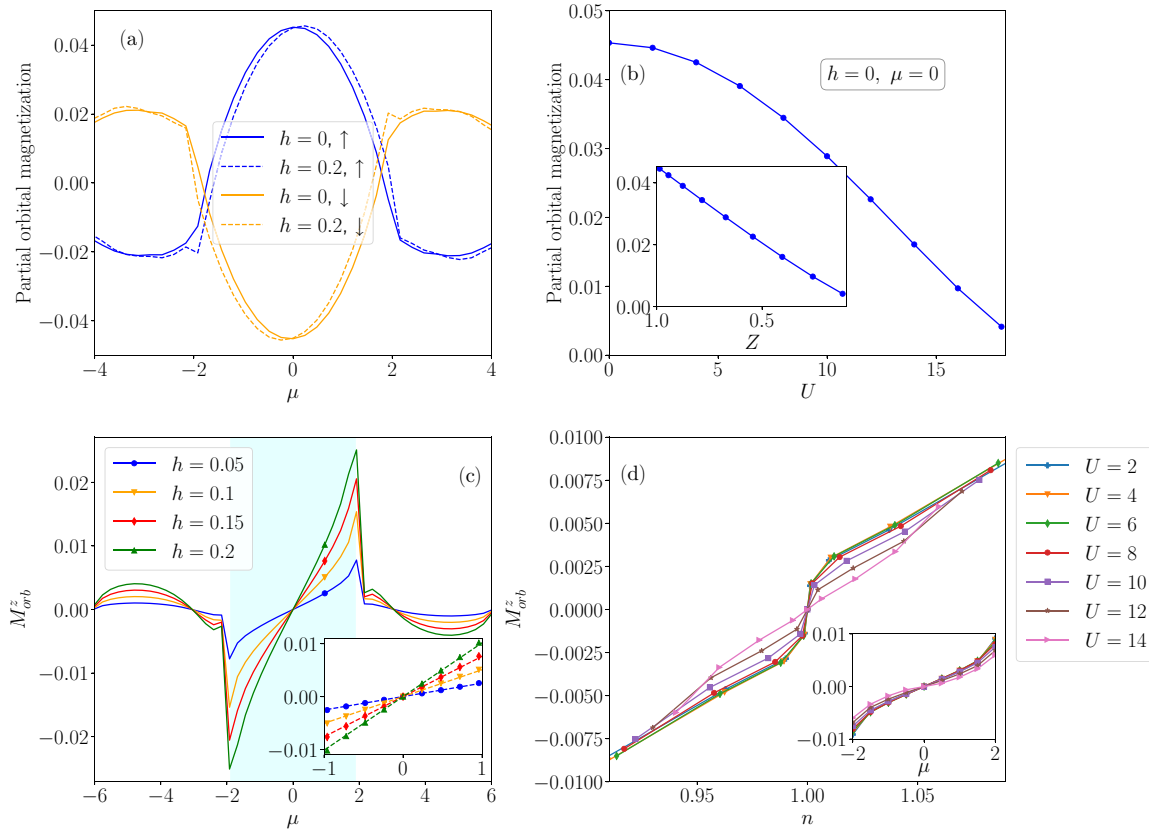

FIG. 3. (a) Noninteracting orbital partial magnetization for $h = 0$ (continuous lines) and $h = 0.2$ (dashed lines) as a function of the chemical potential μ. Note that the partial orbital magnetization is basis dependent and we have chosen the spin basis to represent it. (b) Value of the positive partial orbital magnetization as a function of Hubbard interaction U for $h = 0$ and $\mu = 0$. Interaction renormalizes orbital magnetization via Z as shown in the inset where the positive band orbital magnetization is plotted as a function of the spectral weight. (c) Noninteracting orbital magnetization as a function of chemical potential μ for several values of h. Two regimes are present: the cyan background delimitates the region where bands are mainly linear and white backgrounds where bands have quadratic behavior. The inset is a zoom of the same figure in the linear regime. Marks represent the numerical value from Eq. (12) and dashed lines are the functions $\mu\sigma_{xy}(h)$ with $\sigma_{xy}(h)$ the Hall conductivity in the absence of interaction but with a Zeeman term h. (d) Interacting orbital magnetization as a function of the electronic density near half-filling for $h = 0.05$. The inset is the same plot as a function of chemical potential.

with the Zeeman term h. These symmetry considerations carry over in the interacting case.

In an undoped noninteracting topological insulator, the orbital magnetization is proportional to the Chern number when the chemical potential lies within the energy band gap [9,42]. Indeed, in 2D, a Chern insulator carries a net dissipationless chiral current on its edge that should contribute to the orbital magnetization [8]. Our results show that a similar relationship is valid in a noninteracting ferromagnetic Weyl metal as long as the chemical potential lies in the linearly dispersive band structure, i.e., when $-2 \lesssim \mu \lesssim 2$. Figure 3(c) displays the orbital magnetization of the noninteracting system as a function of chemical potential for several h values. The cyan background delimitates the region where bands are mainly linear. In this region, the orbital magnetization is proportional to the AHE with the chemical potential as coefficient. In other words, for this range of chemical potentials, the following relation holds:

$$M^z_{\text{orb}} = -\mu\sigma_{xy}. \tag{13}$$

Two facts explain this relation. First, for noninteracting systems, it has been shown that, up to fundamental constants, the intrinsic part of the AHE is equal to the derivative of the orbital magnetization with respect to the chemical potential, the Středa formula [14,43]. Second, even if the Fermi energy does not lie on Weyl nodes, as long as the dispersion is still linear and the Fermi surface can be decomposed in disconnected sheets, the anomalous Hall conductivity reduces to its intrinsic value [3] defined in Eq. (10), so that it does not depend on chemical potential. Combining these two results, the orbital magnetization should reduce to Eq. (13). This is verified by the linear behavior of the magnetization near the Fermi energy [cf. Fig. 3(c)]. When the conditions previously enumerated are present, the slope is equal to the anomalous Hall conductivity at half-filling. This argument is not valid for $|\mu| \gtrsim 2$ where nonlinear contributions of the band dispersion are not negligible anymore, marking at the same time the end of the linear behavior of the orbital magnetization.

B. Orbital magnetization for the interacting case

The effect of interactions on the orbital magnetization is complex. In contrast to the AHE, orbital magnetization is not a quantum integer and, therefore, it is not protected against

perturbations. Algebraically, this can be seen by comparing the integrands in Eq. (6), second line, and in Eq. (12). In the anomalous Hall conductivity, the frequency vertex, i.e., the derivative of the inverse Green's function with respect to the Matsubara frequency, plays an important role in making the integrand of the anomalous Hall conductivity interaction independent of spectral weight at low temperature (see Appendix B for a detailed demonstration using the QP approach). This factor is absent in Eq. (12). Figure 3(b) shows the positive band partial orbital magnetization of the half-filled case as a function of U in the absence of h. Upon increasing U, the partial orbital magnetization decreases. This is a consequence of a reduction of the coherent spectral weight, as one can see from the inset of this panel, which shows an almost linear dependence of the positive band partial orbital magnetization on Z. The fact that interaction suppresses the partial orbital magnetization is true for the doped case as well.

On the other hand, we know that interaction enhances the effective Zeeman coupling and, hence, judging from the noninteracting case, it should increase the total orbital magnetization.

Clearly then, interactions introduce two competing mechanisms. Figure 3(d) shows the total orbital magnetization as a function of the electronic density in the Weyl semimetal regime. The magnetization is weakly affected by interaction for $U \lesssim 8$ which means that the two opposing trends almost compensate each other. When U becomes of the same order as the bandwidth ($W = 12$), orbital magnetization becomes more and more sensitive to interactions. They change radically its behavior. The inset in Fig. 3(d) shows the total orbital magnetization as a function of chemical potential. The total orbital magnetization remains linear in μ near half-filling with a slope that is weakly affected by electronic correlations for small U. When $U \approx 12$, deviations start to be visible in the slope of the orbital magnetization.

Because of the presence of the energy vertex and particle-hole symmetry [Eq. (3)], the orbital magnetization is unaffected by the Zeeman term h at $\mu = 0$ for all values of U, as in the noninteracting case.

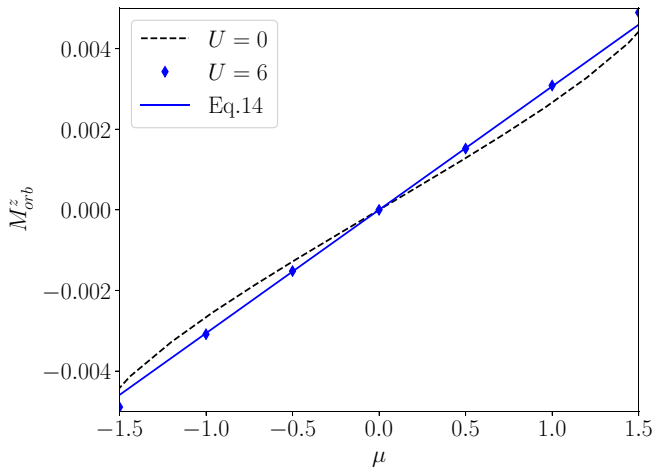

FIG. 4. Comparison between numerical results for the the orbital magnetization and the modified Středa formula (14) where the derivative of Σ' is obtained using a finite-difference method on the self-energy computed to second order in perturbation theory.

In order to check whether or not an equation similar to the Středa formula (13) remains valid in the interacting case, we expand the energy vertex in Eq. (12) with respect to the chemical potential and keep the first order. Then, using the QP Hamiltonian, we obtain

$$M^{\mathrm{QP}}_{\mathrm{orb}} = -\mu Z^2 \left(1 - \frac{1}{2}\frac{\partial \Sigma'}{\partial \mu}\right)\sigma^{\mathrm{QP}}_{xy}, \tag{14}$$

where $\sigma^{\mathrm{QP}}_{xy}$ is the interacting Hall conductivity obtained from the QP approximation. For small to intermediate values of U, the above equation can reproduce quantitatively the change of the orbital magnetization near half-filling, as seen in Fig. 4. In the strong correlation regime, however, the orbital magnetization is not linear anymore, aiming towards zero as we approach the Mott transition.

VI. CONCLUSION

We have studied a Hubbard model of Weyl semimetals on the cubic lattice [23] [Eqs. (1) and (2)] that breaks time-reversal symmetry and parity and that contains four Weyl nodes (Table I). Even in the presence of U, the model is particle-hole symmetric at half-filling [Eq. (3)], whatever the value of the Zeeman term h. The model also has two translated mirror symmetries [Eqs. (4) and (5)], valid for arbitrary interaction and filling when $h = 0$. Within the DMFT framework, we have shown that large enough interactions lead to a transition either to a Mott insulator or to a band insulator. Before these transitions, in the semimetal regime, the anomalous Hall effect and the orbital magnetization are affected very differently by electronic interactions.

Interactions modify the anomalous Hall effect at half-filling by affecting spin polarization when there is a finite Zeeman term h. This physics can be explained with the quasiparticle formalism. Interactions change the effective distance between Weyl nodes and the anomalous Hall effect is still controlled by the distance between nodes in momentum space, as in the noninteracting case. So, even in the presence of a Hubbard U, the topological properties of this Weyl semimetal, at the origin of the intrinsic anomalous Hall effect, are in a sense protected. When $h = 0$, the anomalous Hall effect at half-filling vanishes even in the presence of interactions because the translated mirror symmetries (4) and (5) force the effective Weyl-node separation to be a reciprocal lattice vector.

In contrast with the intrinsic part of the anomalous Hall effect, which involves only the kinetic energy or equivalently the renormalized band structure, the orbital magnetization involves both kinetic and potential energies. In the absence of potential energy, the Středa formula gives a simple relationship between those two quantities. However, Hall conductivity and orbital magnetization are affected differently by interactions. While a quasiparticle approach is sufficient to accurately understand the change in the anomalous Hall conductivity, it fails for the orbital magnetization because of the potential energy contribution.

The orbital magnetization at half-filling vanishes for all U and h as a consequence of particle-hole symmetry [Eq. (3)]. When h is finite, there is a finite orbital magnetization but it is weakly affected by interaction, even if it is *not*

topologically protected. This relative robustness is due to two competing mechanisms: the increase of the anomalous Hall effect due to interaction and the decrease of quasiparticle weight. These effects compensate almost exactly when the chemical potential is not too far from the Weyl nodes. An approach that mixes quasiparticle approach and second-order perturbation theory for the self-energy allowed us to find a modified Středa formula (14) that is accurate for small values of Hubbard interaction. In the strongly correlated regime, the orbital magnetization vanishes due to the interaction-induced localization.

Our work highlights the unusual properties of orbital magnetization and anomalous Hall effect in the presence of interactions. Compounds like the antiferromagnet Mn_3Sn would be interesting to study since the spin magnetization should not dominate over the orbital magnetization.

ACKNOWLEDGMENTS

We thank I. Garate, P. L. S Lopes, P. Rinkel, and S. Bertrand for useful discussions. This work has been supported by the Natural Sciences and Engineering Research Council of Canada (NSERC) under Grant No. RGPIN-2014-04584, the Canada First Research Excellence Fund, and by the Research Chair in the Theory of Quantum Materials. Simulations were performed on computers provided by the Canadian Foundation for Innovation, the Ministère de l'Éducation des Loisirs et du Sport (Québec), Calcul Québec, and Compute Canada.

APPENDIX A: NONINTERACTING HAMILTONIAN AND EFFECTIVE HAMILTONIAN CALCULATION

The noninteracting Hamiltonian breaks time-reversal symmetry and has two bands [cf. Eq. (2)]:

$$\epsilon_{\pm} = \pm\,(h - 2t[\cos(k_x) + \cos(k_y) + \cos(k_z)]^2 + 4t^2\sin^2(k_x) + 4t^2\sin^2(k_y))^{\frac{1}{2}}. \tag{A1}$$

Depending on the value of h, the model exhibits a different number of Weyl nodes. Four Weyl nodes are present in the first Brillouin zone when $|h| < 2t$ while the number of nodes decreases to two when $2t \leqslant |h| < 6t$. The system is fully gapped for large values of h (i.e., $h > 6t$). For this paper, we set $h \ll 2t$. The particle-hole symmetry (3) imposes $\mu = 0$ at half-filling regardless the value of the Zeeman term.

In order to find out the anomalous Hall effect (10), we can use the two low-energy Hamiltonians

$$H^{\text{eff}}_{\pm}(q_x, q_y, k_z) = [h - 2t\cos(k_z)]\boldsymbol{\sigma}_z \pm 2tq_x\boldsymbol{\sigma}_x \mp 2tq_y\boldsymbol{\sigma}_y. \tag{A2}$$

These are low-energy models along the x and y directions, but no approximation is done for the z direction. Each Hamiltonian gives two Weyl nodes located at $k_z = \pm\arccos(h/2t)$ and have the same z component of Berry curvature for the *negative*-energy band:

$$\Omega^z_- = -\frac{2t^2[h - 2t\cos(k_z)]}{\left([h - 2t\cos(k_z)]^2 + 4t^2q_x^2 + 4t^2q_y^2\right)^{\frac{3}{2}}}. \tag{A3}$$

The intrinsic anomalous Hall conductivity of one Weyl node at half-filling where only the *negative*-energy band contributes is

$$\sigma^{\text{eff}}_{xy} = \frac{1}{8\pi^3}\int dk_z d^2q\ \Omega^z_-(q_x, q_y, k_z) \tag{A4}$$

$$= -\frac{1}{8\pi^2}\int_{-\pi}^{\pi} dk_z \text{sgn}[h - 2t\cos(k_z)] \tag{A5}$$

$$= -\frac{1}{2\pi^2}\left[\frac{\pi}{2} - \arccos\left(\frac{h}{2t}\right)\right] \tag{A6}$$

$$= -\frac{1}{2\pi^2}\arcsin\left(\frac{h}{2t}\right). \tag{A7}$$

Here, the function sgn gives the sign of its argument. Since each effective Hamiltonian in Eq. (A2) gives the same result, we finally recover Eq. (10) of the main text.

APPENDIX B: QUASIPARTICLE APPROXIMATION FOR THE LATTICE MODEL

In this Appendix, we derive analytic expressions for the calculation of the anomalous Hall conductivity of the lattice model in the quasiparticle approximation. The quasiparticle Green's function is defined as $\boldsymbol{G}^{\text{QP}} = \mathbf{Z}^{1/2}[i\omega_n\mathbf{I} - \boldsymbol{H}^{\text{QP}}]^{-1}\mathbf{Z}^{1/2} = Z\tilde{\boldsymbol{G}}$ since the spectral weight matrix is diagonal and has identical values for the two spin species. The previous expression is valid for small values of $i\omega_n$, but since the Fermi-surface physics comes from small values of Matsubara frequencies, we expect to find the correct physical expression by using the QP Green's function regardless of the value of the Matsubara frequency.

In this approximation, the expression for the AHE deduced from Eq. (6) becomes

$$\sigma^{\text{QP}}_{xy} = -\text{Im}\frac{1}{\beta}\sum_{\mathbf{k},\omega_n}\text{Tr}\left[v_x\boldsymbol{G}^{\text{QP}}\frac{\partial\boldsymbol{G}^{\text{QP}-1}}{\partial i\omega_n}\boldsymbol{G}^{\text{QP}}v_y\boldsymbol{G}^{\text{QP}}\right] = -\text{Im}\frac{Z^2}{\beta}\sum_{\mathbf{k},\omega_n}\text{Tr}[v_x\tilde{\boldsymbol{G}}\tilde{\boldsymbol{G}}v_y\tilde{\boldsymbol{G}}]. \tag{B1}$$

For simplicity, we omitted the indices $\mathbf{k}$ and $i\omega_n$ in the above expression and used for the vertex $\partial_{i\omega_n}G^{\text{QP}-1} = Z^{-1}$ in the QP approximation. Using the expression for the Green's function and inserting complete sets of states, we find

$$\begin{aligned}\sigma_{xy} &= -\text{Im}\frac{Z^2}{N\beta}\sum_{\mathbf{k},\omega_n}\text{Tr}[v_x\tilde{\boldsymbol{G}}\tilde{\boldsymbol{G}}v_y\tilde{\boldsymbol{G}}] \\ &= -\text{Im}\frac{Z^2}{N\beta}\text{Im}\sum_{\mathbf{k},i\omega_n}\sum_{n,m}\left[\frac{v_x^{n,m}v_y^{m,n}}{\left(i\omega_n - \xi_m^{\text{QP}}\right)^2\left(i\omega_n - \xi_n^{\text{QP}}\right)}\right] \\ &= -\text{Im}\frac{Z^2}{N\beta}\sum_{\mathbf{k},i\omega_n}\sum_{n,m}\left[\frac{\partial}{\partial\xi_m^{\text{QP}}}\left(\frac{v_x^{n,m}v_y^{m,n}}{\left(i\omega_n - \xi_m^{\text{QP}}\right)\left(i\omega_n - \xi_n^{\text{QP}}\right)}\right)\right],\end{aligned} \tag{B2}$$

where $v_i^{n,m}$ is $\langle n|\mathbf{v}_i|m\rangle$, the matrix element n, m of the bare velocity vertex in the band basis, and ξ_n^{QP} are the eigenenergies of the QP Hamiltonian corresponding to the band n. The sum over Matsubara frequencies does not present any issues and,

after some algebra, one finds

$$\sigma_{xy} = -\mathrm{Im}\frac{Z^2}{N}\sum_{\mathbf{k}}\sum_{\substack{n,m\\ m\neq n}}\left[\frac{v_x^{n,m}v_y^{m,n}}{\left(\xi_m^{\mathrm{QP}}-\xi_n^{\mathrm{QP}}\right)^2}\left[n_F\left(\xi_m^{\mathrm{QP}}\right)-n_F\left(\xi_n^{\mathrm{QP}}\right)\right]\right.$$
$$\left.-\frac{v_x^{n,m}v_y^{m,n}}{\xi_m^{\mathrm{QP}}-\xi_n^{\mathrm{QP}}}\frac{\partial n_F\left(\xi_m^{\mathrm{QP}}\right)}{\partial\xi_m^{\mathrm{QP}}}\right]. \tag{B3}$$

At low temperature, the derivative of the Fermi-Dirac distribution can be approximated by a Dirac delta $\delta(\xi_n^{\mathrm{QP}})$, hence, it is only sensitive to the Fermi surface. Since we study a semimetal with the chemical potential lying on the node, we can neglect the corresponding contribution at half-filling. Furthermore, dispersion energies are directly proportional to Z, leading to an expression (B3) that depends on Z only in the Fermi-Dirac distribution since the prefactor Z^2 is canceled out by the renormalization of the band energies appearing in denominators. At low temperature, then, within the QP approximation, it appears that the anomalous Hall conductivity has the same expression as in the noninteracting case with only the replacements $h \to Z(h+\Sigma^z)$ and $t \to Zt$.

[1] N. P. Armitage, E. J. Mele, and A. Vishwanath, Weyl and dirac semimetals in three-dimensional solids, Rev. Mod. Phys. **90**, 015001 (2018).

[2] B. Yan and C. Felser, Topological materials: Weyl semimetals, Annu. Rev. Condens. Matter Phys. **8**, 337 (2017).

[3] A. A. Burkov, Anomalous Hall Effect in Weyl Metals, Phys. Rev. Lett. **113**, 187202 (2014).

[4] S. Ahn, E. J. Mele, and H. Min, Optical conductivity of multi-weyl semimetals, Phys. Rev. B **95**, 161112 (2017).

[5] N. Nagaosa, J. Sinova, S. Onoda, A. H. MacDonald, and N. P. Ong, Anomalous hall effect, Rev. Mod. Phys. **82**, 1539 (2010).

[6] Q. Wang, Y. Xu, R. Lou, Z. Liu, M. Li, Y. Huang, D. Shen, H. Weng, S. Wang, and H. Lei, Large intrinsic anomalous hall effect in half-metallic ferromagnet $Co_3Sn_2S_2$ with magnetic weyl fermions, Nat. Commun. **9**, 3681 (2018).

[7] D. Xiao, J. Shi, and Q. Niu, Berry Phase Correction to Electron Density of States in Solids, Phys. Rev. Lett. **95**, 137204 (2005).

[8] T. Thonhauser, D. Ceresoli, D. Vanderbilt, and R. Resta, Orbital Magnetization in Periodic Insulators, Phys. Rev. Lett. **95**, 137205 (2005).

[9] R. Nourafkan, G. Kotliar, and A.-M. S. Tremblay, Orbital magnetization of correlated electrons with arbitrary band topology, Phys. Rev. B **90**, 125132 (2014).

[10] F. Aryasetiawan, K. Karlsson, and T. Miyake, Green's function theory of orbital magnetic moment of interacting electrons in solids, Phys. Rev. B **93**, 161104 (2016).

[11] J. Shi, G. Vignale, D. Xiao, and Q. Niu, Quantum Theory of Orbital Magnetization and its Generalization to Interacting Systems, Phys. Rev. Lett. **99**, 197202 (2007).

[12] M. Ogata and H. Fukuyama, Orbital magnetism of bloch electrons I. general formula, J. Phys. Soc. Jpn. **84**, 124708 (2015).

[13] M. Ogata, Orbital magnetism of bloch electrons: Ii. application to single-band models and corrections to landau-peierls susceptibility, J. Phys. Soc. Jpn. **85**, 064709 (2016).

[14] P. Streda, Theory of quantised hall conductivity in two dimensions, J. Phys. C: Solid State Phys. **15**, L717 (1982).

[15] P. Hosur and X. Qi, Recent developments in transport phenomena in weyl semimetals, C. R. Phys. **14**, 857 (2013).

[16] K. Kuroda, T. Tomita, M.-T. Suzuki, C. Bareille, A. A. Nugroho, P. Goswami, M. Ochi, M. Ikhlas, M. Nakayama, S. Akebi, R. Noguchi, R. Ishii, N. Inami, K. Ono, H. Kumigashira, A. Varykhalov, T. Muro, T. Koretsune, R. Arita, S. Shin *et al.*, Evidence for magnetic weyl fermions in a correlated metal, Nat. Mater. **16**, 1090 (2017).

[17] S. Nakatsuji, N. Kiyohara, and T. Higo, Large anomalous hall effect in a non-collinear antiferromagnet at room temperature, Nature (London) **527**, 212 (2015).

[18] J. Hofmann, E. Barnes, and S. Das Sarma, Interacting dirac liquid in three-dimensional semimetals, Phys. Rev. B **92**, 045104 (2015).

[19] J. Maciejko and R. Nandkishore, Weyl semimetals with short-range interactions, Phys. Rev. B **90**, 035126 (2014).

[20] B. Roy, P. Goswami, and V. Juričić, Interacting weyl fermions: Phases, phase transitions, and global phase diagram, Phys. Rev. B **95**, 201102 (2017).

[21] W. Witczak-Krempa, M. Knap, and D. Abanin, Interacting Weyl Semimetals: Characterization Via the Topological Hamiltonian and its Breakdown, Phys. Rev. Lett. **113**, 136402 (2014).

[22] M. Laubach, C. Platt, R. Thomale, T. Neupert, and S. Rachel, Density wave instabilities and surface state evolution in interacting weyl semimetals, Phys. Rev. B **94**, 241102 (2016).

[23] S. Roy, M. Kolodrubetz, J. E. Moore, and A. G. Grushin, Chern numbers and chiral anomalies in weyl butterflies, Phys. Rev. B **94**, 161107 (2016).

[24] S. Weinberg, *The Quantum Theory of Fields* (Cambridge University Press, Cambridge, 1995).

[25] A. Georges, G. Kotliar, W. Krauth, and M. J. Rozenberg, Dynamical mean-field theory of strongly correlated fermion systems and the limit of infinite dimensions, Rev. Mod. Phys. **68**, 13 (1996).

[26] M. Caffarel and W. Krauth, Exact Diagonalization Approach to Correlated Fermions in Infinite Dimensions: Mott Transition and Superconductivity, Phys. Rev. Lett. **72**, 1545 (1994).

[27] W. Zhu, D. N. Sheng, and J.-X. Zhu, Magnetic field dependent dynamics and field-driven metal-to-insulator transition of the half-filled hubbard model: A dmft+dmrg study, Phys. Rev. B **96**, 085118 (2017).

[28] R. Nourafkan and G. Kotliar, Electric polarization in correlated insulators, Phys. Rev. B **88**, 155121 (2013).

[29] G. D. Mahan, *Many-Particle Physics*, 2nd ed. (Plenum, New York, 1993).

[30] D. Xiao, M.-C. Chang, and Q. Niu, Berry phase effects on electronic properties, Rev. Mod. Phys. **82**, 1959 (2010).

[31] A. A. Burkov and L. Balents, Weyl Semimetal in a Topological Insulator Multilayer, Phys. Rev. Lett. **107**, 127205 (2011).

[32] K.-Y. Yang, Y.-M. Lu, and Y. Ran, Quantum hall effects in a weyl semimetal: Possible application in pyrochlore iridates, Phys. Rev. B **84**, 075129 (2011).

[33] G. Xu, H. Weng, Z. Wang, X. Dai, and Z. Fang, Chern Semimetal and the Quantized Anomalous Hall Effect in $hgcr_2se_4$, Phys. Rev. Lett. **107**, 186806 (2011).

[34] F. D. M. Haldane, Berry Curvature on the Fermi Surface: Anomalous Hall Effect as a Topological Fermi-Liquid Property, Phys. Rev. Lett. **93**, 206602 (2004).

[35] A. Raoux, M. Morigi, J.-N. Fuchs, F. Piéchon, and G. Montambaux, From Dia- to Paramagnetic Orbital Susceptibility of Massless Fermions, Phys. Rev. Lett. **112**, 026402 (2014).

[36] F. Piéchon, A. Raoux, J.-N. Fuchs, and G. Montambaux, Geometric orbital susceptibility: Quantum metric without berry curvature, Phys. Rev. B **94**, 134423 (2016).

[37] A. Gutiérrez-Rubio, T. Stauber, G. Gómez-Santos, R. Asgari, and F. Guinea, Orbital magnetic susceptibility of graphene and mos_2, Phys. Rev. B **93**, 085133 (2016).

[38] A. Raoux, F. Piéchon, J.-N. Fuchs, and G. Montambaux, Orbital magnetism in coupled-bands models, Phys. Rev. B **91**, 085120 (2015).

[39] M. Ogata, Orbital magnetism of bloch electrons: Iii. application to graphene, J. Phys. Soc. Jpn. **85**, 104708 (2016).

[40] Y. Gao, S. A. Yang, and Q. Niu, Geometrical effects in orbital magnetic susceptibility, Phys. Rev. B **91**, 214405 (2015).

[41] A. Shitade, H. Watanabe, and Y. Yanase, Theory of orbital magnetic quadrupole moment and magnetoelectric susceptibility, Phys. Rev. B **98**, 020407 (2018).

[42] A. Kolchinskaya, P. Komissinskiy, M. B. Yazdi, M. Vafaee, D. Mikhailova, N. Narayanan, H. Ehrenberg, F. Wilhelm, A. Rogalev, and L. Alff, Magnetism and spin-orbit coupling in ir-based double perovskites $la_{2-x}sr_xcoiro_6$, Phys. Rev. B **85**, 224422 (2012).

[43] N. Ito and K. Nomura, Anomalous hall effect and spontaneous orbital magnetization in antiferromagnetic weyl metal, J. Phys. Soc. Jpn. **86**, 063703 (2017).